American Mineralogist, Volume 92, pages 1586–1592, 2007

XRD and HRTEM analyses of stacking structures in sudoite, di-trioctahedral chlorite

Jun Kameda,[1,*] Ritsuro Miyawaki,[2] Ryuji Kitagawa,[3] and Toshihiro Kogure[1]

[1]Department of Earth and Planetary Science, Graduate School of Science, The University of Tokyo, 7-3-1 Hongo, Bunkyo-ku, Tokyo, 113-0033, Japan
[2]Department of Geology, The National Science Museum, 3-23-1 Hyakunin-cho, Shinjuku-ku, Tokyo, 169-0073, Japan
[3]Deparment of Earth and Planetary System Science, Hiroshima University, 1-3-1 Kagamiyama, Higashi-Hiroshima, 739-8526, Japan

Abstract

The stacking structures of sudoite, di-trioctahedral chlorite from two different localities are investigated by powder X-ray diffraction (XRD) and high-resolution transmission electron microscopy (HRTEM). XRD analyses using a Gandolfi camera revealed that the structures of both specimens are similar, corresponding to a one-layer II*bb*-4 (1*A*) polytype. HRTEM observations indicate that the stacking sequence is characterized by a largely uniform intralayer shift of $a/3$ in the $-X_1$ direction (X_i represent the directions along the pseudohexagonal axes) and by an interlayer displacement of similar magnitude in either the $-X_2$ or $-X_3$ direction. Stacking disorder is primarily caused by the mixing of interlayer displacements in the two directions. This disorder is more common in the lath-shaped crystalline specimen from Berezovsk, Russia than in the fine platy crystalline specimen from Ottré, Belgium. DIFFaX simulations of the powder XRD patterns for this stacking model reproduced the observed features well for both specimens. The stacking configuration of these sudoite specimens is considered to be controlled by the corrugation of basal oxygen planes in the 2:1 layer and the corresponding deformation in the brucite-like interlayer sheet.

Keywords: Crystal structure, sudoite, transmission electron microscopy, polytypism

Introduction

Sudoite is a di-trioctahedral Mg-rich and Li-free chlorite with an ideal composition of $(Al_3Mg_2)(Si_3Al)O_{10}(OH)_8$. Sudoite occurs widely, from hydrothermal zones (Hayashi and Oinuma 1964; Billault et al. 2002) to low-grade metamorphic rocks (Fransolet and Bourguignon 1978; Ruiz-Cruz and Sanz de Galdeano 2005). As natural sudoite samples are usually poorly crystalline and fine-grained, it has proven difficult to obtain a complete understanding of the structure of this mineral. Eggleton and Bailey (1967) partially refined the structure of sudoite and confirmed that the mineral is composed of dioctahedral 2:1 layers separated by interlayer trioctahedral brucite-like sheets with a II*bb* stacking sequence.

The stacking structure of a sudoite sample recovered from Ural, Russia was investigated by Drits and Lazarenko (1967) by single-crystal X-ray diffraction (XRD) analysis. The structure thus determined was a regular two-layer structure with a uniform lateral intralayer shift of approximately $a/3$ in the $-X_1$ direction (X_i represent the directions along the pseudohexagonal axes) between the lower and upper tetrahedral sheets of the 2:1 layered structure. In contrast, the interlayer displacement (Kogure et al. 2006a) is shifted by $a/3$ alternately along the $-X_2$ and $-X_3$ directions. A similar stacking structure was also suggested for a sudoite specimen from Ottré, Belgium (Lin and Bailey 1985). Although these studies revealed the basic structure of sudoite, it is not well known whether this two-layer structure is common or what kinds of stacking disorder may be possible.

Direct observation of the stacking sequence in layered materials by high-resolution transmission electron microscopy (HRTEM) is now an invaluable technique for investigating polytypes and disordered stacking sequences. Recently, analyses of several kinds of phyllosilicates for which it has been difficult to acquire HRTEM images due to radiation damage have been performed (e.g., Kogure and Inoue 2005). The stacking sequences indicated by these HRTEM images well explain the powder XRD patterns of pyrophyllite (Kogure et al. 2006a) and talc (Kogure et al. 2006b), leading to definitive determinations of the stacking structures of these minerals. In the present study, HRTEM images are acquired for sudoite to arrive at an accurate characterization of the stacking structures. Although electron diffraction patterns and lattice fringe images have been obtained for sudoite (Abad et al. 2003; Ruiz-Cruz and Sanz de Galdeano 2005), no HRTEM image suitable for direct determination of the stacking structures has been reported. Here, the basic stacking sequence of sudoite and the stacking disorder are determined directly from HRTEM and XRD analyses, and the origin of the relationships is discussed.

Experimental methods

Two sudoite specimens from different localities are examined; a sample from Berezovsk, Ural, Russia consisting of lath-shaped crystals (Drits and Lazarenko 1967), and a sample from Ottré, Belgium comprised of fine platy crystals (Fransolet and Bourguignon 1978). The structural formulas reported for the two specimens are $(Al_{3.03}Mg_{1.89}Fe_{0.24})_{\Sigma 5.16}(Si_{3.15}Al_{0.85})_{\Sigma 4}O_{10}(OH)_8$ (Jige et al. 2003) and

* E-mail: kameda@eps.s.u-tokyo.ac.jp

$(Al_{2.84}Mg_{1.91}Fe^{3+}_{0.19}Mn_{0.02})_{\Sigma 4.96}(Si_{3.01}Al_{0.99})_{\Sigma 4}O_{10}(OH)_8$ (Fransolet and Bourguignon 1978), respectively.

XRD measurements were performed using a 114.6 mm diameter Gandolfi camera under Ni-filtered Cu$K\alpha$ radiation. The specimens were several hundred micrometers in size, fixed to a thin glass fiber. The patterns were recorded on an imaging plate and processed using a Fuji BAS-2500 bio-imaging analyzer and a computer program developed by Nakamuta (1999). Simulations of powder XRD patterns were performed using DIFFaX (Treacy et al. 1991), in which the diffraction patterns are calculated from layered materials considering various stacking sequences.

Specimens for TEM observations were prepared by a method similar to that described in Kogure (2002). The powdered specimen was embedded in epoxy resin between two glass slides. After hardening, the glass slides were cut using a diamond wheel to laths of ca. 1 mm thick. The laths were thinned to ca. 50 μm by mechanical grinding, and then finished by argon ion milling. HRTEM was performed at 200 kV using a JEOL JEM-2010 microscope with a nominal point resolution of 0.2 nm (C_s = 0.5 mm). Degradation of the sudoite specimen under electron radiation occurs very rapidly, permitting only one exposure for the acquisition of HRTEM images at magnifications of 400000× or 500000×. Up to 10 images were successfully obtained for each specimen; each recorded on film and digitized using a charge-coupled device (CCD) camera for image processing. Noisy contrast due to amorphous phases on the specimen surface was removed by background subtraction filtering (Kilaas 1998) implemented in Gatan Digital Micrograph version 3.1. Simulations of HRTEM contrast were performed by a multi-slice method using Mac-Tempas (Kilaas 1991).

Results and discussion

XRD analysis of sudoite

Figure 1a shows the observed XRD patterns of the sudoite specimens from Berezovsk and Ottré, and powder XRD patterns calculated assuming a monoclinic two-layer structure (2*M*) and triclinic one-layer polytype (1*A*). It is known that six different interlayer stacking sequences are possible in chlorite (I*aa*, I*ab*, I*bb*, II*aa*, II*ab*, and II*bb*), depending on the interlayer inclination of the brucite-like sheet with respect to the octahedral sheet in the 2:1 layer, and also the geometry of hydrogen bonding between basal oxygen and hydroxyl (Bailey 1988). This interlayer stacking sequence can be recognized from the peak positions and intensity distribution of $k = 3n$ reflections in the XRD pattern (Bailey 1988). The pattern for the 2*M* structure with II*bb* sequence was calculated using the crystallographic parameters reported by Aleksandrova et al. (1973). The positions and relative intensities of the $k = 3n$ peaks simulated assuming the 2*M* structure generally agree well with the observed positions, suggesting that the interlayer stacking sequence in the two specimens is II*bb*, as reported in previous work (Eggleton and Bailey 1967; Shirozu and Higashi 1976).

However, there are notable dissimilarities between the observed patterns and the patterns calculated for 2*M*. Figure 1b shows a magnified region for the 2θ range of 18–33°. Careful scrutiny of the patterns reveals that several broad and relatively weak peaks exhibited by the present specimens are not reproduced by the 2*M* model, as indicated by broken lines in the figure. However, these observed peaks are well reproduced by calculations considering a triclinic one-layer polytype (1*A*). The 1*A* model was calculated using the atomic positions of clinochlore II*bb*-4 (Joswig and Fuess 1990) with a vacant M1 site in the 2:1 layer, and the cell dimensions (*a*, *b*, and d_{002}) of sudoite 2*M*. The II*bb*-4 stacking sequence involves an angle of $2/3\pi$ between the intralayer shift and interlayer displacement. The stacking sequence of the 1*A* (II*bb*-4) polytype thus appears to be dominant in both samples, accompanied by a certain degree of disorder. Comparison of the two observed patterns indicates that the stacking in the Berezovsk sample is more heavily disordered than in the Ottré sample.

The splitting of several of the $k = 3n$ peaks can be attributed to significant deviation of the α angle from zero, and/or cosβ being not equal to $-a/3c$ in the 1*A* unit cell. However, the cell dimensions could not be refined further for the present specimens due to difficulty in precise determination and indexing of peak positions as a result of the subtle splitting.

HRTEM analysis of stacking sequence in sudoite

Figure 2a shows a bright-field image of the Ottré sudoite specimen observed slightly oblique to the [100] direction. Iijima and Buseck (1978) and Kogure and Nespolo (1999) reported that the stacking disorder in mica can be clearly observed if the crystal is observed at a slight angle from the zone axes. Figure 2a reveals an irregular banded contrast parallel to the layers, indicative of a disordered stacking structure. Figures 2b and 2c show the corresponding selected-area electron diffraction (SAED) patterns along the $[3\bar{1}0]$ and [100] directions. The $[3\bar{1}0]$ pattern displays discrete spots at 0.71 nm^{-1} intervals along the 13*l* reciprocal lattice row. Considering the XRD results, this pattern indicates that the stacking is fully composed of the II*bb* sequence. On the other hand, the [100] pattern is almost completely coincident with that for the 1*A* polytype, the only difference being a streak along the 02*l* row suggestive of stacking disorder.

Figure 3 shows simulated HRTEM contrast images and the corresponding crystal structures of sudoite viewed along the three directions according to the atomic parameters of sudoite 2*M* (Aleksandrova et al. 1973). In these images, both the intralayer shift and interlayer displacement can be identified by the relative positions of distinctive black spots in the 2:1 layer, each of which corresponds to a pyroxene-like tetrahedral chain in the beam direction. White bars connect the two closest black spots in the lower and upper tetrahedral sheets within the 2:1 layer, and the inclination of the bar reliably indicates the intralayer shift in each 2:1 layer. Using the nomenclature of Baronnet (1992), zero, dextral (positive), and sinistral (negative) shift are denoted by "0", "+", and "–," The stagger of the white bar in the upper 2:1 layer from that in the lower layer, corresponding to interlayer displacement, is expressed similarly.

Figures 4a–4c show three representative HRTEM images of the Berezovsk sudoite. The contrast for all 2:1 layers is consistent with the simulated contrast in the [100] direction (Fig. 3), indicating that the intralayer shift is uniform and parallel (or anti-parallel) to the beam direction. In Figure 4c, several 2:1 layers with a different intralayer shift are present, but such disorder is not common in the specimen. The interlayer displacement is largely uniform, demonstrating that the interlayer stacking sequence is II*bb*-4 (assuming II*bb*). Zero shift, that is, when the interlayer displacement is parallel to the intralayer shift (II*bb*-2 stacking sequence), occurs rarely. Dextral (+) interlayer displacement is pervasive in Figure 4a, forming domains with 1*A* stacking sequence consistent with the XRD results. In Figure 4b, however, the populations of dextral and sinistral shift are comparable. A domain with two-layer periodicity involving regular alternation of the interlayer displacements can be seen in this example. This

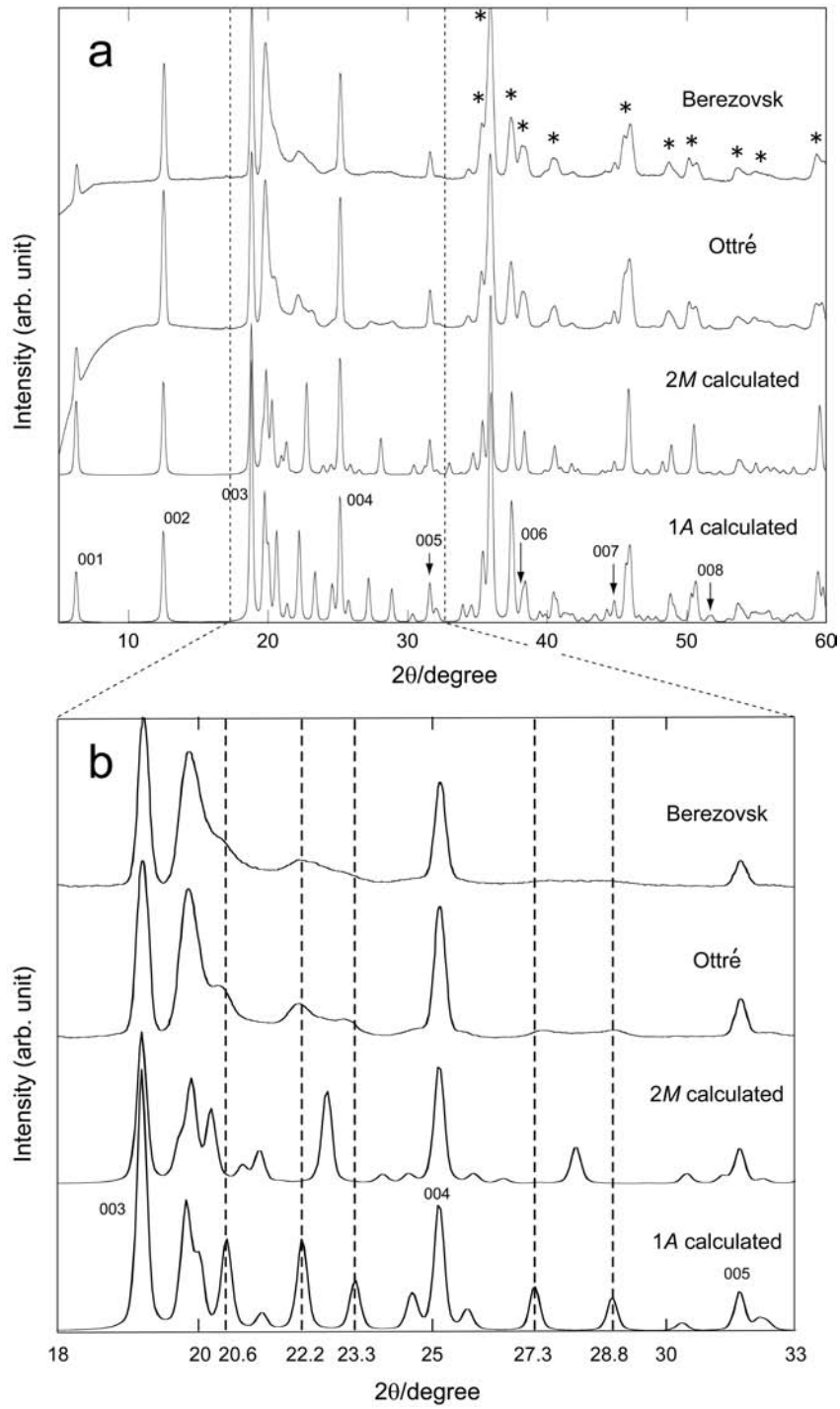

FIGURE 1. (**a**) XRD patterns of Berezovsk and Ottré sudoite. (**b**) Magnified patterns in the 2θ range of 18–33°. Calculated patterns for sudoite 2*M* and 1*A* polytypes are also shown. Peaks marked with asterisks (*) are $k = 3n$ reflections.

structure corresponds to the sudoite-2*M* polytype as reported in previous work. However, the occurrence of such a structure is quite rare in this specimen. It is thus proposed that the intralayer shift is relatively uniform in the $-X_1$ direction, and that stacking disorder is caused mainly by the mixing of interlayer displacements in the $-X_2$ and $-X_3$ directions.

Figure 4d shows a HRTEM image of the Ottré specimen in the same orientation as shown in Figures 4a–4c. Interlayer displacement is uniform throughout apart from a small region of zero shift as stacking disorder. Interlayer displacement along

the $-X_1$ direction corresponds to sinistral shift (–) in this case, while $-X_2$ and $-X_3$ displacement appear as zero and dextral shift, respectively. The stacking structure is thus essentially equivalent to that in the Berezovsk specimen, corresponding to 1*A* dominant stacking. The stacking disorder is also a mixture of the directions of interlayer displacement along the $-X_2$ and $-X_3$ directions, as in the Berezovsk sample. Overall, the Ottré specimen displays less stacking disorder than the Berezovsk specimen.

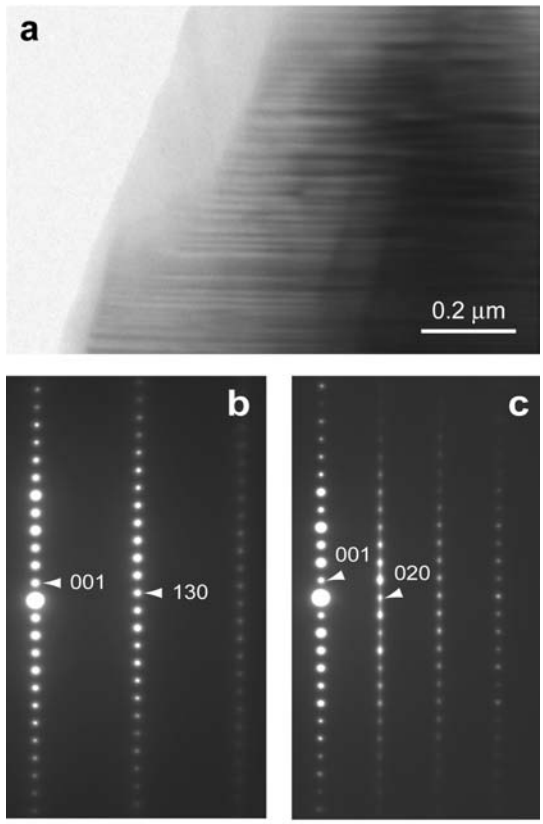

FIGURE 2. (**a**) Bright-field image of Ottré specimen observed subparallel to [100], and corresponding SAED patterns observed parallel to (**b**) [3$\bar{1}$0] and (**c**) [100]

DIFFaX simulation of XRD patterns of sudoite

XRD simulations of sudoite were conducted to examine whether the stacking structures observed in the HRTEM images are representative of the bulk specimens. For simplification, disorder of intralayer shift in the 2:1 layers and interlayer displacement parallel to the intralayer shift (II*bb*-2 sequence) are ignored. The total shift between the adjacent unit layers is expressed by the sum of intralayer shift and interlayer displacement. In the present case, the intralayer shift is approximately $a/3$ in the $-X_1$ direction, and interlayer displacement is close to $a/3$ in the $-X_2$ or $-X_3$ direction. Consequently, the total shift is $a/3$ in the $+X_2$ or $+X_3$ direction. The crystallographic parameters of sudoite reported by Aleksandrova et al. (1973) were used in the simulation, where the total shift is expressed as $-0.175\mathbf{a} + 0.16\mathbf{b}$ in the $+X_2$ direction or $-0.175\mathbf{a} - 0.16\mathbf{b}$ in the $+X_3$ direction.

In DIFFaX program employed for simulations (Treacy et al. 1991), the stacking sequence is expressed by a matrix (α_{ij}) of the probability that layer-type *j* succeeds layer-type *i*. Simulations are performed for two cases, with total shift in either the $+X_2$ or $+X_3$ direction. The stacking sequence is expressed by a 2×2 matrix, defined according to the probability *p* that the same interlayer displacement occurs between adjacent layers (Kogure et al. 2006a), i.e.,

$$\alpha_{11} = p,\ \alpha_{12} = 1 - p$$
$$\alpha_{21} = 1 - p,\ \alpha_{22} = p$$

If $p = 1.0$, the simulated stacking sequence is the ideal 1*A* polytype. If $p = 0$, the stacking sequence is a perfect 2*M* polytype as proposed in previous work. If $p = 0.5$, the stacking sequence is a random mixture of the two types of interlayer displacement. Figure 5 shows the results of XRD simulation as a function of *p*. A

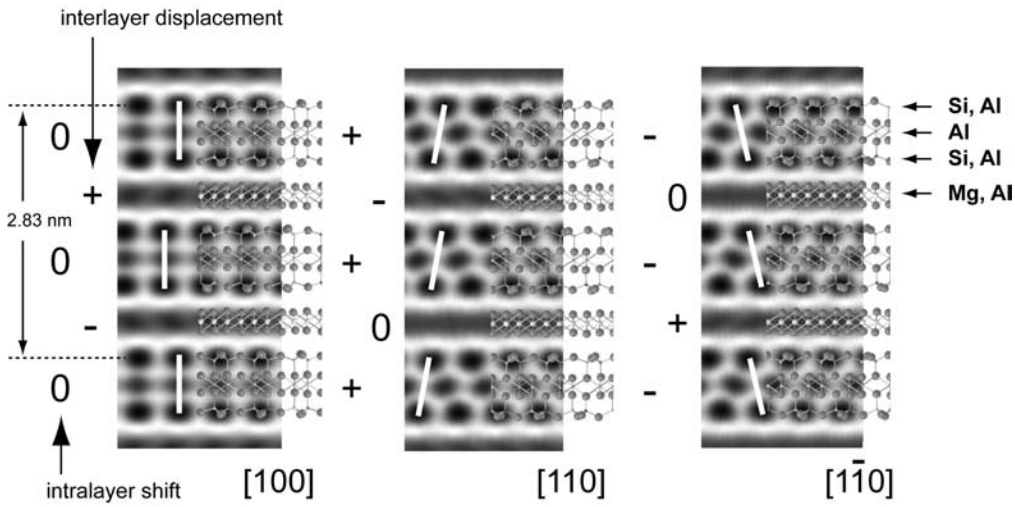

FIGURE 3. Simulated HRTEM contrast images and corresponding crystal structure of sudoite 2*M* observed parallel to [100], [110], and [1$\bar{1}$0]. White bars connect closest black spots in lower and upper tetrahedral sheets within the 2:1 layer. Orientation of offset is marked as zero (0), dextral (+), or sinistral (–).

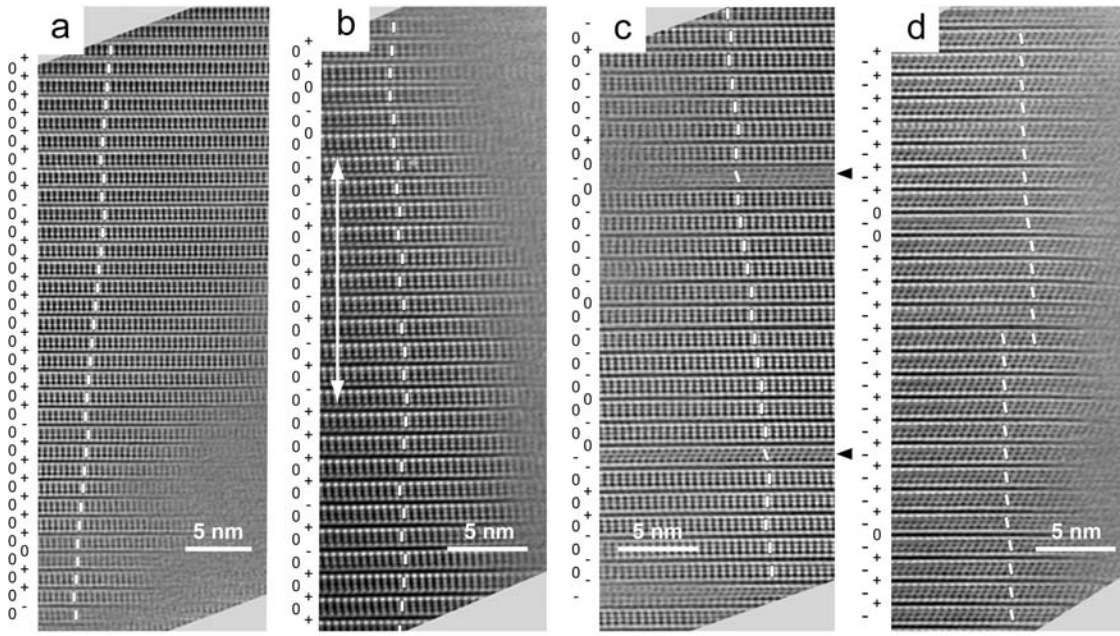

FIGURE 4. (**a**–**c**) Filtered HRTEM images of Berezovsk sudoite observed parallel to X_1 showing 1*A* dominant stacking. A two-layer periodic structure is indicated by an arrow in **b**, and 2:1 layers with different intralayer shifts are marked by arrows in **c**. (**d**) Filtered HRTEM image of Ottré sudoite parallel to X_2 and X_3.

p value of 0.6 or slightly higher reproduces the Berezovsk pattern well, whereas $p = 0.7$ reproduces the characteristics of the Ottré pattern. The probability for the same interlayer displacement to persist into the succeeding layer is therefore approximately twice that of the occurrence of a different displacement. The HRTEM observations clearly support this result (Figs. 4a and 4d).

Factors controlling the stacking sequence in sudoite

The present sudoite stacking structures are very similar to those reported for diagenetic kaolinite (Kogure and Inoue 2005) and pyrophyllite (Kogure et al. 2006a). The largely uniform orientation of unit layers and alternation of interlayer displacement in two directions, the main features of stacking disorder, are common in minerals containing a dioctahedral sheet. Kogure et al. (2006a) suggested that the interlayer stacking structure in pyrophyllite is controlled by the corrugation of basal oxygen planes in the 2:1 structure, which occurs due to tilting of the silicate tetrahedra to form a large trans-vacant octahedral site in the dioctahedral sheet. To minimize oxygen-oxygen repulsion across the interlayer and bring the two adjacent layers closer, the intralayer shifts in the adjacent layers will be aligned in the same direction, parallel to the corrugation, and the interlayer displacement will occur in different directions to the intralayer shift.

Corrugation of the basal oxygen plane is also expected in sudoite. However, the basal oxygen atoms bridging the interlayer region are not in contact as in pyrophyllite, but form hydrogen bonds with hydroxyls in the brucite-like sheet. If the brucite-like sheet maintains trigonal symmetry and the surface hydroxyl planes are flat in sudoite, the same intralayer shift across the interlayer will not occur.

Aleksandrova et al. (1973) performed a structural refinement

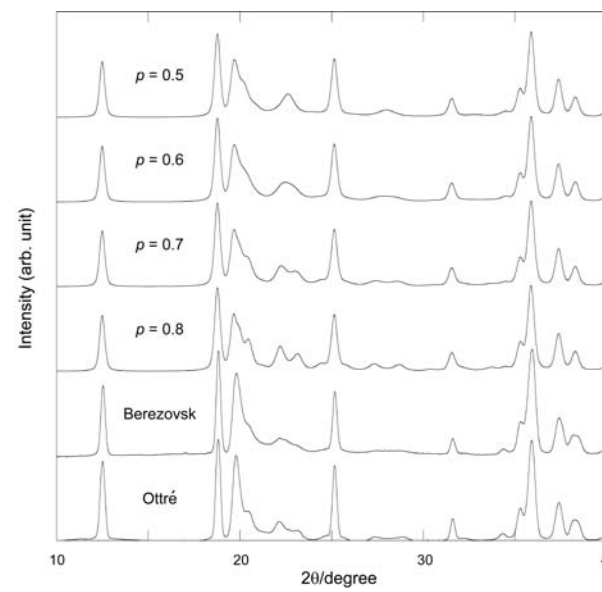

FIGURE 5. Simulated XRD patterns ($2\theta = 10$–$40°$) for various *p* values. Observed XRD patterns for both sudoite specimens are also shown.

for sudoite 2*M*, as shown in Figure 6. The structure of clinochlore is shown for comparison (Joswig and Fuess 1990). Although the *R* value for the refinement was not small (0.138), the corrugation of basal oxygen atoms can be clearly observed parallel to the intralayer shift. There is also a slight variance of the heights of hydroxyls (0.13 Å) in the brucite-like sheet, partially offsetting the fluctuation in OH-O distances caused by the corrugation

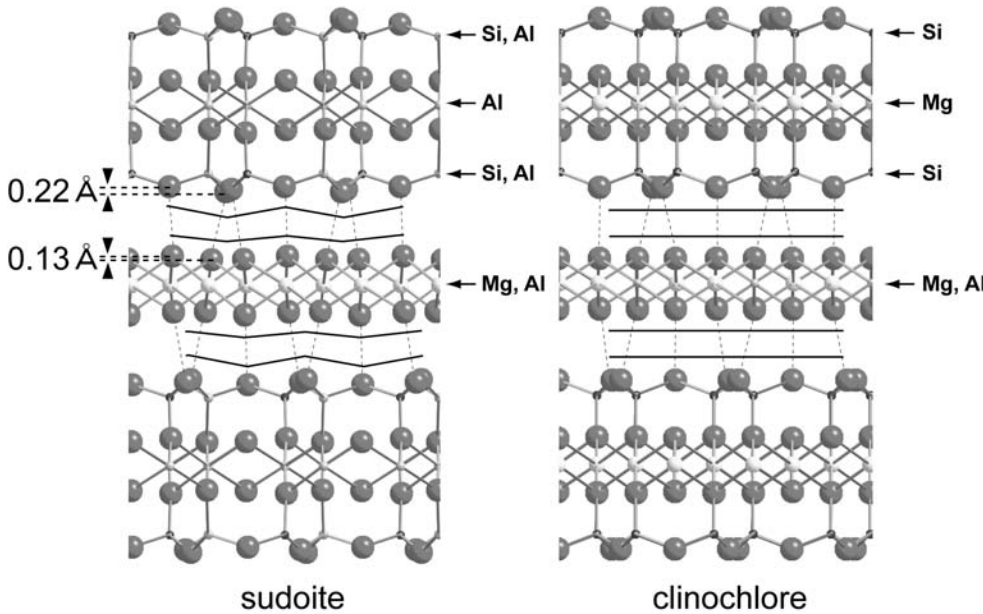

FIGURE 6. Crystal structures of sudoite and clinochlore based on the data of Aleksandrova et al. (1973) and Joswig and Fuess (1990), respectively, showing the corrugation of basal oxygen planes in the 2:1 layer and the deformation of hydroxyl planes of the brucite-like sheet.

of basal oxygen. If the lower and upper hydroxyl planes in the brucite-like sheet have the same atomic arrangement (as in Fig. 6), it is preferable that the intralayer shifts of the adjacent 2:1 layers will be aligned in the same direction. Similarly, the II*bb*-2 stacking sequence is less favorable than the II*bb*-4 stacking if the deformation in the brucite-like sheet is present in sudoite.

The factors controlling the selection of the 1*A*, 2*M*, or disordered sequence are not obvious. Lin and Bailey (1985) reported sudoite-2*M* from the same locality. However, our powder XRD measurement using a conventional diffractometer and a larger powder volume than that for the Gandolfi camera showed a similar pattern (data are not shown), indicating that disordered 1*A* is the dominant polytype. According to surface topographic studies of sudoite from Berezovsk (Jige et al. 2003), the crystallization of sudoite is thought to have occurred by a two-dimensional nucleation mechanism and not by spiral growth. Nevertheless, spiral growth can also be initiated by the imperfectly oriented attachment of different grains (Penn and Banfield 1998). Even the longer-period polytypes, which are thermodynamically less stable, can be formed in the model proposed by Penn and Banfield (1998). This model may explain the origin of sudoite 2*M*. The degree of the disorder by the two directions of the interlayer displacement is likely to be related to the effects of growth temperature, analogous to pyrophyllite (Eberl 1979; Kogure et al. 2006a).

ACKNOWLEDGMENTS

The authors are grateful to S. Guggenheim (University of Illinois, Chicago) for donating the sudoite specimens. Appreciation is also extended to T. Takeshige (University of Tokyo) for preparation of TEM specimens. Electron microscopy was performed at the Electron Microbeam Analysis Facility of the Department of Earth and Planetary Science, University of Tokyo. This work was supported in part by a Grant-in-Aid (no. 17340160, Section B) from the Japan Society for the Promotion of Science (JSPS). One of the authors (J.K.) was financially supported by a JSPS Research Fellowship for Young Scientists.

REFERENCES CITED

Abad, I., Nieto, F., Peacor, D.R., and Velilla, N. (2003) Prograde and retrograde diagenetic and metamorphic evolution in metapelitic rocks of Sierra Espuña (Spain). Clay Minerals, 38, 1–23.

Aleksandrova, V.A., Drits, V.A., and Sokolova, G.V. (1973) Crystal structure of ditrioctahedral chlorite. Kristallografiya, 18, 81–88.

Bailey, S.W. (1988) X-ray diffraction identification of the polytypes of mica, serpentine and chlorite. Clays and Clay Minerals, 36, 193–213.

Baronnet, A. (1992) Polytypism and stacking disorder. In P. Buseck, Ed., Minerals and reactions at the atomic scale: Transmission electron microscopy, 27, 231–288. Reviews in Mineralogy, Mineralogical Society of America, Chantilly, Virginia,

Billault, V., Beaufort, D., Patrier, P., and Petit, S. (2002) Crystal chemistry of Fe-sudoite from uranium deposits in the Athabasca Basin (Saskatchewan, Canada). Clays and Clay Minerals, 50, 70–81.

Drits, V.A. and Lazarenko, E.K. (1967) Structural-mineralogical characteristics of donbassite. Mineralgicheskii Sbornik, 21, 40–48.

Eberl, D. (1979) Synthesis of pyrophyllite polytypes and mixed layers. American Mineralogist, 64, 1091–1096.

Eggleton, R.A. and Bailey, S.W. (1967) Structural aspects of dioctahedral chlorite. American Mineralogist, 52, 673–689.

Fransolet, A.M. and Bourguignon, P. (1978) Di/trioctahedral chlorite in quartz veins from the Ardennes, Belgium. Canadian Mineralogist, 16, 365–373.

Hayashi, H. and Oinuma, K. (1964) Aluminian chlorite from Kamikita mine, Japan. Clay Science, 2, 22–30.

Iijima, S. and Buseck, P.R. (1978) Experimental study of disordered mica structure by high-resolution electron microscopy. Acta Crystallographica, A34, 709–719.

Jige, M., Kitagawa, R., Zaykov, V.V., and Sinyakovskaya, I. (2003) Surface microtopography of sudoite. Clay Minerals, 38, 375–382.

Joswig, W. and Fuess, H. (1990) Refinement of a one-layer triclinic chlorite. Clays and Clay Minerals, 38, 216–218.

Kilaas, R. (1991) HREM image simulation. In G.W. Bailey, Ed., Proceeding of 49th EMSA meeting, p. 45–51. San Francisco Press, California.

——— (1998) Optical and near-optical filters in high-resolution electron microscopy. Journal of Microscopy, 190, 45–51.

Kogure, T. (2002) Investigation of micas using advanced TEM. In A. Mottana, F.P. Sassi, J.B. Thompson, Jr., S. Guggenheim, Eds., Micas: Crystal Chemistry and Metamorphic Petrology, 46, p. 281–312. Reviews in Mineralogy and Geochemistry, Mineralogical Society of America, Chantilly, Virginia.

Kogure, T. and Inoue, A. (2005) Determination of defect structure in kaolin minerals by high-resolution transmission electron microscopy (HRTEM). American Mineralogist, 90, 85–89.

Kogure, T. and Nespolo, M. (1999) A TEM study of long-period mica polytypes:

determination of the stacking sequence of oxybiotite by means of atomic resolution images and Periodic Intensity Distribution (PID). Acta Crystallographica, B55, 507–516.

Kogure, T., Jige, M., Kameda, J., Yamagishi, A., and Kitagawa, R. (2006a) Stacking structures in pyrophyllite revealed by high-resolution transmission microscopy (HRTEM). American Mineralogist, 91, 1293–1299.

Kogure, T., Kameda, J., Matsui, T., and Miyawaki, R. (2006b) Stacking structures in disordered talc: interpretation of its X-ray diffraction pattern. American Mineralogist, 91, 1363–1370.

Lin, C.Y. and Bailey, S.W. (1985) Structural data for sudoite. Clays and Clay Minerals, 33, 410–414.

Nakamuta, Y. (1999) Precise analysis of a very small mineral by a X-ray diffraction method. Journal of Mineralogical Society of Japan, 28, 117–121 (in Japanese with English abstract).

Penn, R.L. and Banfield, J.F. (1998) Imperfect oriented attachment: Dislocation generation in defect-free nanocrystals. Science, 281, 969–971.

Ruiz-Cruz, M.D. and Sanz de Galdeano, C. (2005) Compositional and structural variation of sudoite from the Betic cordillera (Spain): A TEM/AEM study. Clays and Clay Minerals, 53, 639–652.

Shirozu, H. and Higashi, S. (1976) Structural investigations of sudoite and regularly interstratified sericite/sudoite. Mineralogical Journal, 8, 158–170 (in Japanese with English abstract).

Treacy, M.M.J., Newsam, J.M., and Deem, M.W. (1991) A general recursion method for calculating diffracted intensities from crystals containing planar fault. Proceedings of the Royal Society of London A, 433, 499–520.

Manuscript received August 6, 2006
Manuscript accepted May 21, 2007
Manuscript handled by Warren Huff